Processing and Application of Ceramics 14 [3] (2020) 210–217
https://doi.org/10.2298/PAC2003210P

High pressure and high temperature behaviour of TiAlN coatings deposited on *c*-BN based substrates

Robert Pilemalm[1,*], Anna Sjögren[2]

[1]*Thin Film Physics Division, Department of Physics, Chemistry and Biology (IFM), Linköping University, SE-581 83 Linköping, Sweden*
[2]*Element Six AB, SE-915 32 Robertsfors, Sweden*

Received 28 April 2020; Received in revised form 29 June 2020; Accepted 8 July 2020

Abstract

High pressure and high temperature experiments with a Hall belt apparatus of cathodic arc deposited $Ti_{0.63}Al_{0.37}N$ and $Ti_{0.37}Al_{0.63}N$ on polycrystalline cubic BN substrate reveal a strong influence of pressure on the decomposition rate of TiAlN. The pressure induces enhanced phase stability while keeping the interfaces between coatings and the substrates intact. Hardness measurements of the as-deposited coatings and after high-pressure high-temperature treatment show that the hardness after treatment of $Ti_{0.63}Al_{0.37}N$ at 5.35 GPa, 1300 °C and after 66 min drops from 29.6 to 27.8 GPa, because after this treatment this sample contains cubic TiN and hexagonal AlN. This drop is much smaller than if the coatings are just heat treated at 1300 °C and suggests that an enhancement of TiAlN-coatings on cubic BN cuttings tools can be achieved by increasing the pressure/stress during cutting. For $Ti_{0.37}Al_{0.63}N$ treated at 5.35 GPa, 1300 °C and after 66 min the hardness drops from 36.1 to 28.6 GPa, which means that the coating has first decomposed through spinodal decomposition and one of products of this decomposition has further phase transformed and the final products are cubic TiN and hexagonal AlN.

Keywords: *cubic boron nitride, Hall belt apparatus, high-pressure high-temperature, spinodal decomposition, TiAlN*

I. Introduction

Cubic (*c*) $Ti_{x-1}Al_xN$ coatings have been used as protective coatings for cutting and machining applications since the first reports of positive effects when adding Al to TiN in 1980 [1,2]. Addition of Al results in improved oxidation resistance [3], thermal stability and hardness [4,5] making $Ti_{x-1}Al_xN$ coatings beneficial for applications such as machining and turning of steel for instance [1,2,4,6]. When the cutting inserts are coated, the main idea is that productivity should increase. The improved hardness is due to the age hardening phenomenon resulting from isostructural spinodal decomposition of *c*-TiAlN into nanometer sized TiN- and AlN-rich domains [6,7]. Spinodal decomposition of *c*-TiAlN has been reported to occur at elevated temperatures (800–1000 °C) [8] but also during machining [9]. However, *c*-AlN is not thermodynamically stable and transforms by nucleation and growth to its stable phase, hexagonal (*h*) AlN, if the temperature is increased further [10].

The formation of *h*-AlN results in a drastic hardness drop. Attempts to delay the detrimental transformation to *h*-AlN have proven successful in terms of alloying TiAlN with for instance Cr [11], V [12], and Zr [13], through a design of the coating architecture in the form of a TiAlN/TiN or a TiAlN/CrN multilayer with layers a few nm thick [14,15], and by introducing nitrogen vacancies [16]. An effect of improving the thermal stability of the protective coating of cutting tools is that the substrate also must be able to sustain higher temperatures. Cemented carbide (WC/Co) is the most commonly used substrate material. At temperatures above 1300 °C Co diffusion from the substrate into the film occurs, which deteriorates the mechanical properties [4,6]. A hard material with better thermal stability is polycrystalline boron nitride (PCBN), which is a composite consisting of *c*-BN and a ceramic binder that potentially could replace WC/Co substrates for the new and more

* Corresponding author: tel: +46 737210085,
e-mail: *robert.pilemalm@gmail.com*

thermally stable TiAlN-based coatings. Non-deposited cubic boron nitride is competing with diamond and is increasingly used for technical applications such as hard turning [17,18]. Part of this study is to evaluate if any reactions occur between PCBN and TiAlN at high pressure and high temperature (HPHT) and parts are related to how the combination of high temperature and high pressure affects the decomposition of TiAlN. To invoke pressure in the analysis is based on the fact that during metal cutting the coating is exposed to external mechanical loads that may exceed 2 GPa [9]. Furthermore, experimental and theoretical studies suggest that a combination of high temperature and high pressure promotes the favourable spinodal decomposition and suppresses the detrimental *h*-AlN formation [19–22]. These former experimental studies were performed on TiAlN powders at considerably higher pressures (8–14 GPa). Here, we extend the pressure range and study the decomposition process in TiAlN when attached to a substrate such that we can report hardness. We have chosen two alloy compositions, $Ti_{0.63}Al_{0.37}N$ and $Ti_{0.37}Al_{0.63}N$, which at room temperature are located inside the spinodal. According to a phase diagram that includes lattice vibration by Shulumba *et al.* [23] the composition $Ti_{0.37}Al_{0.63}N$ is unstable up to approximately 1700 °C while $Ti_{0.63}Al_{0.37}N$ is stable above ~1200 °C. The work by Alling *et al.* [8] suggests that the alloy composition most affected by pressure is close to $Ti_{0.63}Al_{0.37}N$ in terms of a shift of the spinodal to higher temperatures. Considering AlN, the pressure-temperature phase diagram [21] implies that *h*-AlN is always more stable than *c*-AlN for pressures less than 8 GPa, but the difference decreases with increasing pressure and temperature. In this paper we report how the decomposition of arc evaporated TiAlN coatings deposited on PCBN-substrates and HPHT treated at different temperatures at 5 GPa affects hardness. The results show that TiAlN/PCBN interface remains intact even after exposure to 5.35 GPa and 1300 °C and that the decomposition rate is decreased at 5.35 GPa compared to ambient pressure for the $Ti_{0.63}Al_{0.37}N$ alloy.

II. Experimental

The used PCBN-substrates consist of *c*-BN ~90 vol% and 10 vol% binder material being primarily different types of oxides. The substrates were shaped into discs with a radius of 18 mm and a height of 3.2 mm and mechanically polished to a mirror-like finish. Cathodic arc deposition with 63 mm in diameter TiAl-compound cathodes was conducted in an industrial scale Sulzer/Metaplas MZR-323 deposition system in a 4.5 Pa N_2 atmosphere. During deposition a negative substrate bias of 30 V was applied, and the substrate temperature was kept at 450 °C. In order to alter the chemical composition of the coatings, cathodes with different compositions, $Ti_{0.60}Al_{0.40}$ and $Ti_{0.33}Al_{0.67}$ were used. Prior to inserting the substrates in the chamber, they were degreased in an industrial cleaning line consisting of ultrasonic baths with alkali and alcohol solutions. Thereafter the substrates were mounted on a single rotating fixturing drum at the same height as the centre of the cathode. For more details regarding the geometry of the substrate mounting see ref [9]. The substrates were sputter cleaned for 20 min with Ar ions just before initiating deposition. The compositions of the coatings were determined with an energy dispersive X-ray spectrometer (EDX) attached to a Leo 1550 Gemini scanning electron microscope (SEM). For compositional analysis the SEM was operated with an acceleration voltage of 20 kV and for imaging at 5 kV.

The HPHT experiments were performed at Element Six in Robertsfors in Sweden with a Hall belt apparatus, that generates high pressure by pushing two anvils together using pistons and that press was originally designed for synthesizing diamond [24], but can also be used to study behaviour of materials under different conditions [25] as in the case of this study. The Hall belt apparatus owned by Element Six that was used in this study is normally used to produce *c*-BN from *h*-BN through a HPHT-induced phase transformation. The mechanically generated pressure of the press is finally transmitted through a pressure medium to a sample capsule, which is resistively heated [26]. The sample in the Hall belt apparatus is well isolated from the surroundings like air in the facility, where it is situated. The design of the used specimen capsule is schematically illustrated in Fig. 1. The separation discs were put in place to facilitate sample recovery after high-pressure high-temperature (HPHT) treatment. The inside surfaces of the capsule that was in contact with the film during the experiments were spray coated with an Al_2O_3-TiO_2 mixture to prevent reactions with the Nb-cup. Each high-pressure high-temperature treatment batch contained four capsules. All high-pressure high-

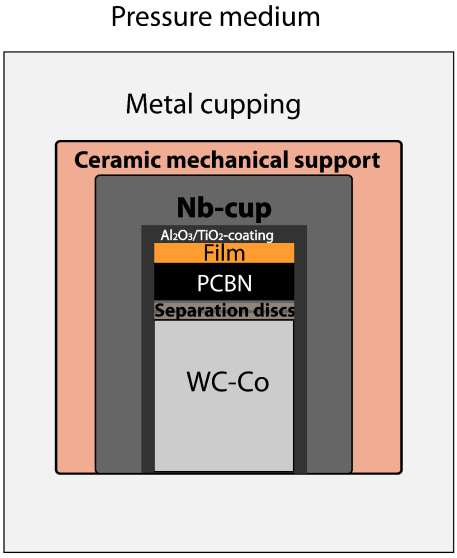

Figure 1. Illustration of the capsule that contained the samples during HPHT experiments

temperature treatments were conducted at a constant pressure of 5.35 ± 0.15 GPa while the temperature and duration were varied between 1050 and 1300 °C, and 6 to 66 min, respectively. The pressure was applied at room temperature followed by a temperature ramp-up to half of the required power in 2 min and then an additional 10 min to reach maximum temperature. During cooling the power was decreased to half in 6 min and to zero after additional 11 min.

The samples were recovered by crushing the capsule followed by sand blasting. Some residues of the Al_2O_3/TiO_2 mixture were not removed in order not to jeopardize the coating.

Isothermal annealing was performed in a Sintevac furnace from GCA Vacuum industries using a holding time of 2 h. The annealing experiment was done at atmospheric pressure in flowing Ar in order to avoid oxidation and at the temperatures 1050 and 1300 °C.

X-ray diffractometry (XRD) was performed with a diffractometer in Bragg-Brentano geometry (θ-2θ scan) using Cu-Kα radiation (PANalytical Empyrean; United Kingdom). Cross-sectional transmission electron microscopy (TEM)-samples were prepared with a focused ion beam system (FIB) (Carl Zeiss Crossbeam EsB; Germany) using a lift-out method suggested by Langford and Petford-Long [27]. TEM was performed with an accelerating voltage of 200 kV which was equipped with a high angle annular dark field detector for STEM, an (EDX) detector and an electron energy loss spectrometer (EELS) (FEI Tecnai G^2 20 UT microscope, United States of America). A nanoindenter equipped with a contact area calibrated Berkovich diamond tip was used for hardness measurements (UMIS Nanoindentor; Germany). The values reported here are the average hardness extracted from 40 indents using the method by Oliver and Pharr [28]. The maximum load used was 45 mN, which yielded penetration depths always less than 250 nm while the thicknesses of $Ti_{0.63}Al_{0.37}N$ coating is 4 μm and of the $Ti_{0.37}Al_{0.63}N$ coating it is 2.5 μm. In some cases it was not possible to obtain reliable data due to the remaining residues of the encapsulation or fragmentation during sample recovery after HPHT treatment.

III. Results and discussion

The compositions of the as-deposited films as determined by EDX are $Ti_{0.63}Al_{0.37}N$ and $Ti_{0.37}Al_{0.63}N$, respectively. A slight decrease in the Al/Ti ratio compared to the cathode composition is to be expected for coatings grown by arc deposition due to the preferential resputtering of Al [29].

Figures 2(a-c) show cross-sectional bright field (BF) transmission electron micrographs together with SAED patterns of $Ti_{0.63}Al_{0.37}N$ for the as-deposited sample (Fig. 2a), the HPHT treated samples at 5.35 GPa and 1050 °C for 6 min (Fig. 2b) and 1300 °C for 66 min (Fig. 2c), respectively. The as-deposited sample displays a columnar microstructure with columns growing coarser away from the substrate, consistent with often observed growth mode with a nucleation zone next to the substrate and then competitive growth between grains of different crystallographic orientations [30,31]. The SAED pattern shows a cubic crystal structure without any traces of a hexagonal phase. The HPHT treated sample at 5.35 GPa and 1050 °C for 6 min also displays a columnar microstructure and a cubic structure, i.e. SAED shows no traces of a hexagonal phase in the coating. The column boundaries are more distinct, which is caused by vacancies and interstices being annihilated in accordance with what has been observed previously for heat-treated arc deposited coatings [6]. The sample exposed to a HPHT at 1300 °C for 66 min displays an altered microstructure with large grains next to the film surface while the grain next to the substrate remains fine. In this sample a phase transformation is evident in the coating since the SAED pattern shows the presence of both cubic and hexagonal phases i.e. *c*-TiN and *h*-AlN. Even though diffusion is apparent in the coating during HPHT treatment, the substrate/coating interface remains intact even at the most severe HPHT condition, i.e. no new phases have formed next to the interface. Additional elemental analysis based on EELS in the vicinity of the interface between the PCBN substrate and the $Ti_{0.63}Al_{0.37}N$ coating shows no diffusion of B or Ti across the interface.

Figure 3a shows a BF micrograph of the as-deposited $Ti_{0.37}Al_{0.63}N$ sample. It has a finer columnar structure with smaller grains compared to the $Ti_{0.63}Al_{0.37}N$ sample. The grains are also here coarser further away from the substrate, but with a smaller variation in grain size. The SAED pattern confirms that the structure of the film is cubic. The HPHT treated samples with 1050 °C for 6 min (Fig. 3b) have more distinct grains. In contrast to $Ti_{0.63}Al_{0.37}N$ it also contains *h*-AlN.

Figure 2d is a higher magnification STEM micrograph of the $Ti_{0.63}Al_{0.37}N$ coating after HPHT treatment at 1050 °C for 6 min together with an inserted elemental map based on EDX. The elemental map reveals segregation of Ti (green) and Al (red) compared to the as-deposited sample (not shown here), where the elements are homogeneously distributed. Figure 2e is a high resolution TEM (HRTEM) image of the same area with the electron beam along the [001] zone axis, showing a cubic lattice. Figure 2f shows a STEM micrograph of the 1300 °C 66 min treated $Ti_{0.63}Al_{0.37}N$ sample together with an element map inset. The mass contrast in the micrograph reveals domains consisting of the heavier (Ti) element (darker areas) and the lighter (Al) element (brighter areas) consistent with the inserted elemental map. Based on the SAED pattern in Fig. 2c the Al-rich areas are dominated by *h*-AlN and compared to the 1050 °C for 6 min HPHT treated sample, the domains have grown significantly larger. The top layer is Pt from the processing with FIB. In addition to the Pt-layer and the TiAlN-coating two layers with TiO_2

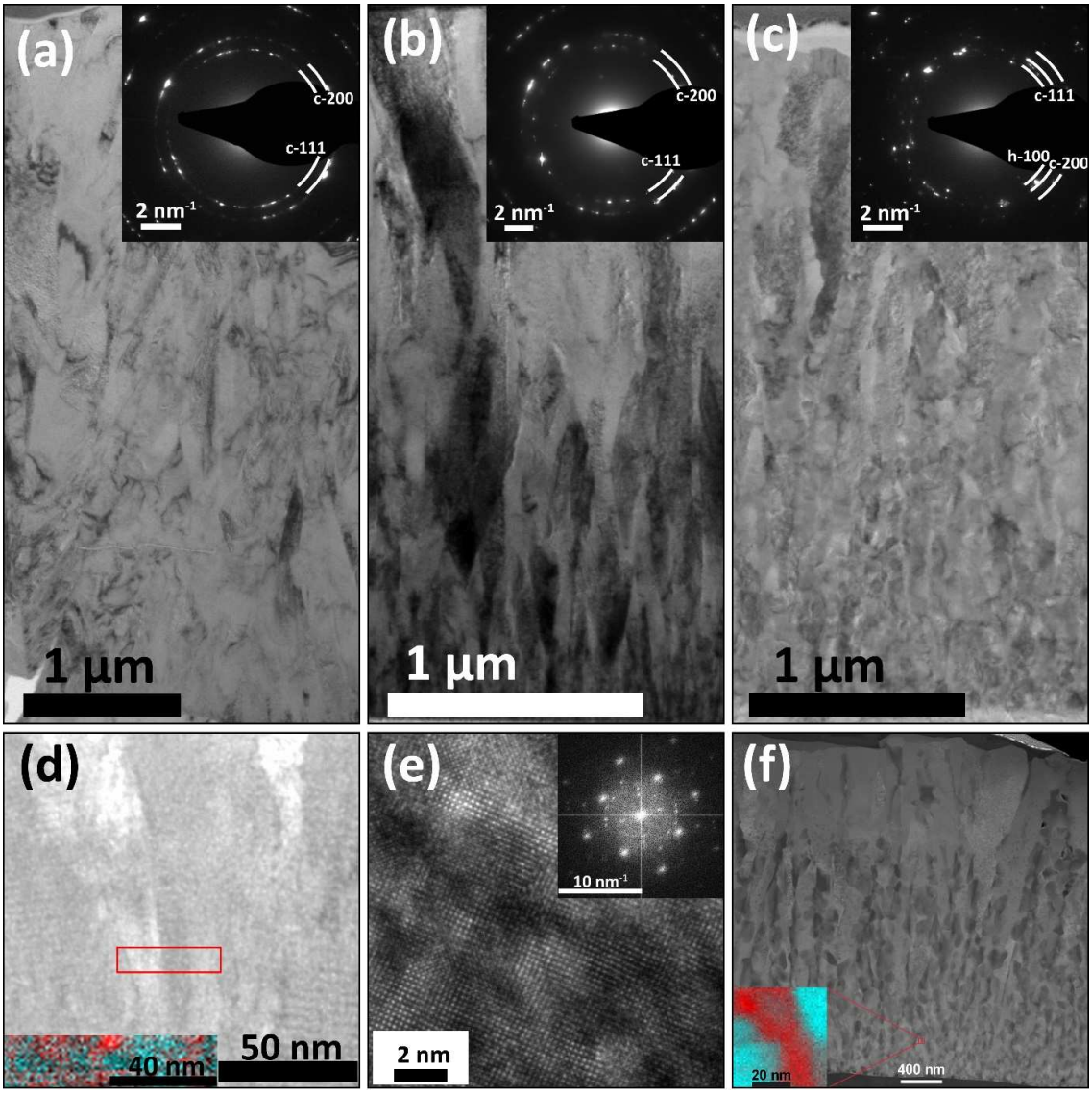

Figure 2. Cross-sectional bright field transmission electron micrographs of $Ti_{0.63}Al_{0.37}N$ a) for as-deposited state, b) after HPHT treatment, 5.35 GPa and 1050 °C for 6 min, c) after HPHT treatment, 5.35 GPa and 1300 °C for 66 min, d) scanning transmission electron micrographs of $Ti_{0.63}Al_{0.37}N$ after HPHT treatment, 5.35 GPa and 1050 °C for 6 min, e) high resolution transmission electron micrograph of $Ti_{0.63}Al_{0.37}N$ at 5.35 GPa and 1050 °C for 6 min, f) scanning transmission electron micrograph of $Ti_{0.63}Al_{0.37}N$ at 5.35 GPa and 1300 °C for 66 min

and of Al_2O_3 on top of the coating can be seen. Figure 3c shows the corresponding elemental map for the $Ti_{0.37}Al_{0.63}N$ sample after HPHT treatment at 1050 °C for 6 min and also here a segregation between Ti (green) and Al (red) is evident. The HRTEM micrograph in Fig. 3d with the beam along the [011] zone axis is from an Al-rich area, revealing that it has a hexagonal structure.

Figure 4a shows X-ray diffractograms of the $Ti_{0.63}Al_{0.37}N$ coating after different HPHT treatments. The as-deposited coating has a cubic NaCl structure with a lattice parameter of approximately 4.19 Å. The *c*-$Ti_{0.63}Al_{0.37}N$ 200 peak and the substrate *c*-BN 111 peak overlap. The peaks from AlB_2 and AlB_{12} (labeled "s") and *h*-AlN all originate from the binder material in the PCBN substrate, since no *h*-AlN was detected in the coating by SAED-TEM. HPHT treatment at a temperature of 1050 °C for 6 min results in a shift of the *c*-TiAlN peaks towards higher angles corresponding to a new lattice parameter of approximately 4.18 Å accompanied with a marginal increase of the full width at half maximum (FWHM).

The diffractogram after HPHT treatment at 1050 °C for 66 min (Fig. 4a) shows more narrow peaks close to the positions for pure *c*-TiN. At this stage TiN and AlN have segregated and the NaCl-structured phase is now TiN-rich, labeled as *c*-Ti(Al)N. No *c*-AlN is detected and instead a shoulder has evolved on the *h*-AlN 100 peak. It suggests formation of small domains of *h*-AlN in the coating with a slightly different lattice parameter compared to the *h*-AlN in the substrate. The difference in lattice parameter stems from semicoherent interfaces between *c*-TiAlN and *h*-AlN [21]. At the higher temperature, 1300 °C, and longer times this shoulder has disappeared in line with a strain

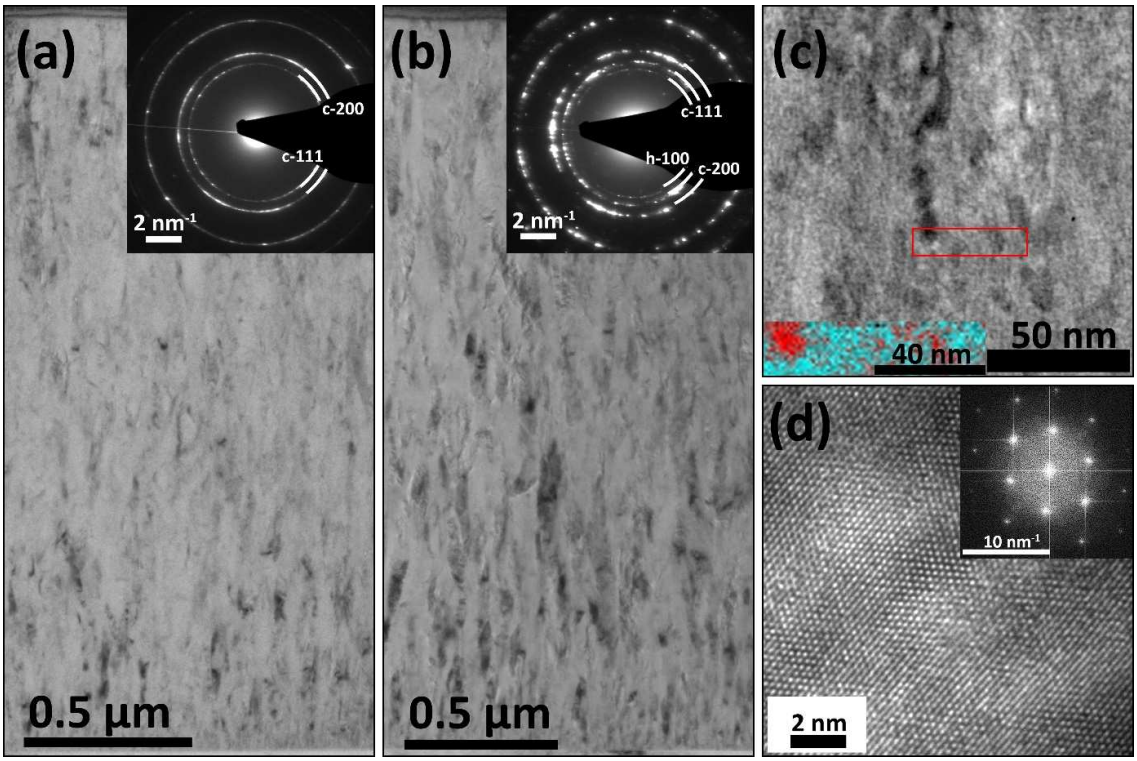

Figure 3. Cross-sectional bright field transmission electron micrographs of $Ti_{0.37}Al_{0.63}N$: a) for as-deposited state, b) after HPHT treatment, 5.35 GPa and 1050 °C for 6 min, c) scanning transmission electron micrographs of $Ti_{0.37}Al_{0.63}N$ after HPHT treatment, 5.35 GPa and 1050 °C for 6 min, d) high resolution transmission electron micrograph of $Ti_{0.37}Al_{0.63}N$ at 5.35 GPa and 1050 °C for 6 min

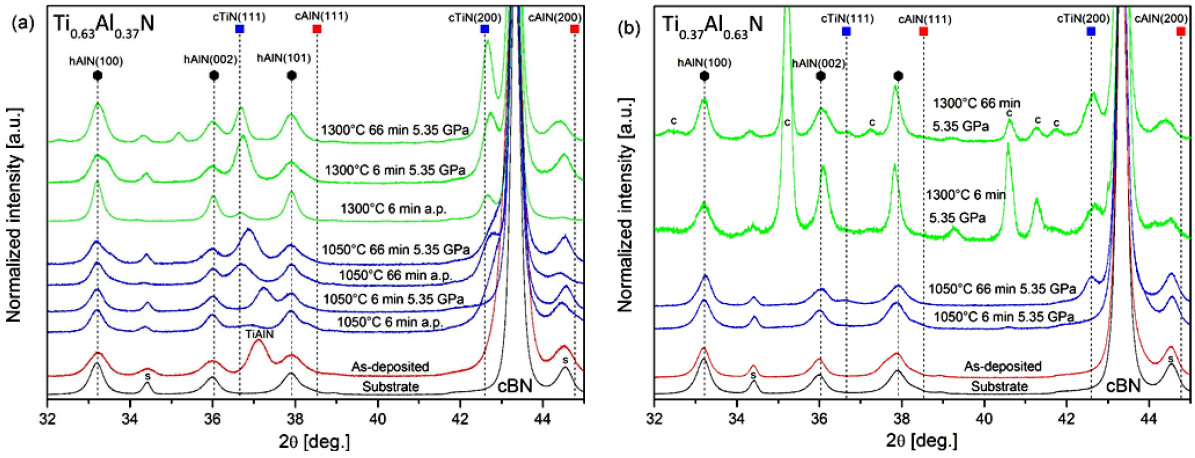

Figure 4. X-ray diffractograms of as-deposited state and after different HPHT treatments of: a) $Ti_{0.63}Al_{0.37}N$ and b) $Ti_{0.37}Al_{0.63}N$

relaxed *h*-AlN. The diffractograms of the HPHT treated samples are considerably different from the ones obtained from heat-treated samples at 1050 °C and ambient pressure. After heat treatment for 6 min a considerable broadening of the 200 peak has occurred. Due to the overlap with a strong substrate *c*-BN peak the entire peak cannot be resolved. However, broadening is of the same magnitude as the one of the HPHT-sample after 66 min suggesting a more rapid process and perhaps a different decomposition path-way at ambient pressure. When $Ti_{0.63}Al_{0.37}N$ is heat-treated at ambient pressure for 66 min the TiN 200 peak is apparent. The presence of semicoherent *h*-AlN has been observed for the samples heat-treated at ambient pressure, which is in contrast to the HPHT treated samples. In fact, the segregation behaviour of specimen annealed at ambient pressure display behaviour more consistent with nucleation and growth while HPHT treatment results in spinodal decomposition.

In addition, slight oxidation has occurred with formation of Al_2O_3, which is the same oxide previously reported to form during high temperature treatment of TiAlN at ambient pressure [3].

The other alloy composition, $Ti_{0.37}Al_{0.63}N$, is located well inside the miscibility gap for all temperatures considered here. For $Ti_{0.37}Al_{0.63}N$ it is well established that

Table 1. Measured hardness of as-deposited state and after HPHT treatment under different conditions (* means that it was not possible to measure the hardness, because the Nb-cup was not possible to remove after the tests)**

Sample	Hardness [GPa]	
	$Ti_{0.63}Al_{0.37}N$	$Ti_{0.37}Al_{0.63}N$
As-deposited	29.6 ± 1.3	36.1 ± 1.7
5.35 GPa, 1050 °C, 6 min	32.3 ± 1.4	32.3 ± 1.7
5.35 GPa, 1050 °C, 66 min	31.7 ± 1.2	***
5.35 GPa, 1300 °C, 6 min	29.3 ± 1.3	***
5.35 GPa, 1300 °C, 66 min	27.8 ± 1.0	28.6 ± 1.2

spinodal decomposition occurs when it is heat-treated at ambient pressures [7]. This process primarily occurs at lower temperatures than 1050 °C and already after 6 min about 40% of the *c*-AlN has transformed to *h*-AlN [10]. Hence, X-ray diffractograms of this alloy composition heat treated at ambient pressure are not presented. Instead, Fig. 4b only shows HPHT treated samples. The samples exposed to the highest temperature 1300 °C show traces of the protective spray coating (marked "c") corresponding to Al_2O_3 and TiO_2 and the high temperature phase Al_2TiO_5 [32]. Due to the difference in chemical composition the *c*-$Ti_{0.37}Al_{0.63}N$ 111 peak is overlapping with the *h*-AlN substrate peak causing an asymmetric peak around 38° in the as-deposited coating. It has been experimentally shown that the unstrained lattice parameter for this composition should be 4.14 Å [33] which results in an overlap of the 200 peak with an intense *c*-BN peak at $2\theta \sim 43.7°$. After HPHT treatment for 6 min at 1050 °C this peak broadens. For samples exposed to a HPHT treatment at 1050 °C for 66 min and 1300 °C the presence of *c*-TiN is even more apparent. In these cases it is not possible to distinguish the expected *h*-AlN in the film from the *h*-AlN in the substrate suggesting an incoherent *h*-AlN similar to what has been seen for heat treatment at ambient pressures.

Table 1 shows the measured hardness of the studied samples. After HPHT treatment at 1050 °C for 6 min of the $Ti_{0.63}Al_{0.37}N$ coating, there is an increase in hardness from 30 GPa for the as-deposited case to 32 GPa. Increased hardness after annealing has been reported before [34]. The reason is the formation of coherent cubic domains with different elastic properties due to spinodal decomposition, c.f. Fig. 2e. More extended HPHT treatments of the same film for longer times or higher temperatures result in hardness decrease. In all these cases *h*-AlN has formed. Here, it can be noted that the main reason for the drop of hardness is due to the fact that *h*-AlN has formed. Other factors that can affect the hardness in general are for instance composition, growth conditions and microstructure [35]. In the cases of the two studied compositions and where *h*-AlN has formed, the morphology of the coatings after the tests has changed as well.

The STEM image in Fig. 2d and its elemental map show that there has been a decomposition of the original $Ti_{0.63}Al_{0.37}N$ coating after HPHT treatment at 1050 °C for 6 min. Figure 2e suggests that the domains are coherent, which is expected in cases of isostructural spinodal decomposition [6,21,36]. In the case of the coating at ambient pressure the microstructure is fully segregated with incoherent *h*-AlN, i.e. a more advanced stage of decomposition. The decomposition of TiAlN is diffusion controlled [30]. Given that both ambient and high-pressure treatments result in the same decomposition path-way the metal diffusion at 5 GPa must be considerably slower than at ambient pressure. The diffusivities of Ti and Al in TiAlN as a function of pressure are unknown, but it is known that for solids higher pressure implies denser molecule packing, which in turn means smaller free-path length and hence slower diffusion. On the other hand and from a thermodynamic point of view, the driving force for decomposition should increase with increasing pressure since the spinodal shifts to higher temperatures when the pressure is increased [8]. A different scenario is that the decomposition pathways differ between anneals at ambient and high pressures resulting in different decomposition rates. The alternative decomposition route is precipitation of *h*-AlN through nucleation and growth directly from *c*-TiAlN. This mechanism would require that the two anneals occur on opposite sides of the spinodal. Calculations by Shulumba *et al.* [23] suggest that this is possible for the alloy with low Al-content but not for the one with high Al-content. The hardness of the as-deposited samples is in agreement with what has been reported previously for arc deposited TiAlN of similar compositions [4]. The expected age hardening after isothermal annealing is not observed for $Ti_{0.37}Al_{0.63}N$ due to over ageing at the conditions studied here, i.e. formation of *h*-AlN. However, a significant hardness increase is seen for $Ti_{0.63}Al_{0.37}N$ at 1050 °C after 6 min conforming to the well-established fact that formation of microstructure consisting of nanometre sized *c*-TiN and *c*-AlN coherent domains results in an increased hardness [4–6,20,34]. Perhaps an even higher hardness can be obtained if the anneal is extended longer than 6 min but less than 66 min.

Furthermore, it has been reported that for the same TiAlN-PCBN coating-substrate systems the adhesion was lower compared to using a more commonly used cemented carbide substrate when tested in their as-deposited states [37]. Here, we observe by visual inspection and from TEM images that the TiAlN coating remains adhered to PCBN even after a HPHT treatment at 5.35 GPa and 1300 °C. This is of technological interest since PCBN is used as a cutting tool for machining

of alloys containing iron. It is known that the presence of Fe may cause BN to oxidize and form B_2O_3, which in turn leads to chemical degradation [38]. The result that TiAlN does not react with PCBN during HPHT treatment, its oxidation resistance gained by the formation of Al_2O_3 [3], and the improved mechanical properties due to spinodal decomposition indicate that the TiAlN coating delays the time before the PCBN gets in contact with the work piece material. This means that even though the coating is softer than the substrate we expect it to delay the degradation during machining, which have been verified by the fact that the efficient tool life of PCBN tools coated with TiAlN and other coatings has significantly increased compared to non-coated PCBN tools [39]. The degradation in the context of this article is expected to be slower due to the fact that no chemical interaction between coating and substrate has occurred, which is an interesting result for other similar studies.

IV. Conclusions

We have used a Hall belt apparatus to perform simultaneous high pressure high temperature (HPHT) studies of $Ti_{0.63}Al_{0.37}N$ and $Ti_{0.37}Al_{0.63}N$ deposited on polycrystalline boron nitride (PCBN) at different conditions, which were compared to as-deposited and annealed samples. It has been shown ex situ that the decomposition of TiAlN is slower at high pressure compared to ambient pressure. In addition, no chemical interactions between TiAlN and PCBN were observed (XRD and EELS map) up to 5.35 GPa and 1300 °C. TiAlN has the potential to protect a PCBN substrate during metal machining due to the high chemical integrity. Hardness measurements of the two coatings as-deposited and ex situ measured after high-pressure high temperature treatment show that the hardness after treatment of $Ti_{0.63}Al_{0.37}N$ and $Ti_{0.37}Al_{0.63}N$ at 5.35 GPa, 1300 °C and after 66 min drops from 29.6 and 36.1 GPa to 27.8 and 28.6 GPa, respectively. The samples after this treatment contain *c*-TiN and *h*-AlN instead of the original solid TiAlN solutions.

Acknowledgements: This work was funded by the Swedish Knowledge Foundation (KK-stiftelsen) and by the VINNEX Center of Excellence for Functional Nanoscale Materials (FunMat). The technical support doing the HPHT experiments by Richard Rönnholm, Lars-Ivar Nilsson and Åke Andersin at Element six AB is acknowledged. Finally, Lars Hultman and Jianqiang Zhu are acknowledged for valuable discussion and support all through the project.

References

1. H.A. Jehn, S. Hoffman, V.E. Rückborn, W.D. Münz, "Morphology and properties of sputtered (Ti,Al)N layers on high speed steel substrates as a function of deposition temperature and sputtering atmosphere", *J. Vac. Sci. Technol. A*, **4** (1986) 2701–2705.
2. O. Knotek, M. Böhmer, T. Leyendecker, "On structure and properties of sputtered Ti and Al based hard compound films", *J. Vac. Sci. Technol. A*, **4** (1986) 2695–2700.
3. B.J. Kim, Y.C. Kim, J.W. Nah, J.J. Lee, "High temperature oxidation of $(Ti_{1-x}Al_x)N$ coatings made by plasma enhanced chemical vapor deposition", *J. Vac. Sci. Technol. A*, **17** (1999) 133–137.
4. A. Hörling, L. Hultman, M. Odén, J. Sjölen, L. Karlsson, "Mechanical properties and machining performance of $Ti_{1-x}Al_xN$-coated cutting tools", *Surf. Coat. Technol.*, **191** (2005) 384–392.
5. R. Rachbauer, S. Massl, E. Stergar, D. Holec, D. Kiener, J. Keckes, J. Patscheider, M. Stiefel, H. Leitner, P.H. Mayrhofer, "Decomposition pathways in age hardening of Ti-Al-N films", *J. Appl. Phys.*, **110** (2011) 023515.
6. A. Hörling, L. Hultman, M. Odén, J. Sjölen, L. Karlsson, "Thermal stability of arc evaporated high aluminum-content $Ti_{1-x}Al_xN$ thin films", *J. Vac. Sci. Technol. A*, **20** (2002) 1815–1823.
7. A. Knutsson, M.P. Johansson, P.O. Persson, L. Hultman, M. Odén, "Thermal decomposition products in arc evaporated TiAlN/TiN multilayers", *Appl. Phys. Lett.*, **93** (2008) 143110.
8. B. Alling, M. Odén, L. Hultman, I. Abrikosov, "Pressure enhancement of the isostructural cubic decomposition in $Ti_{1-x}Al_xN$", *Appl. Phys. Lett.*, **95** (2009) 181906.
9. N. Norrby, M.P. Johansson, R. M'Saoubi, M. Odén, "Pressure and temperature effects on the decomposition of arc evaporated $Ti_{0.6}Al_{0.4}N$ coatings incontinuous turning", *Surf. Coat. Technol.*, **209** (2012) 203–207.
10. N. Norrby, L. Rogström, M.P. Johansson-Jõesaar, N. Schell, M. Odén, "In-situ X-ray scattering study of the cubic to hexagonal transformation of AlN in $Ti_{1-x}Al_xN$", *Acta Mater.*, **73** (2014) 205–214.
11. H. Lind, R. Forsén, B. Alling, N. Ghafoor, F. Tasnádi, M.P. Johansson, I.A. Abrikosov, M. Odén, "Improving thermal stability of hard coating films via a concept of multicomponent alloying", *Appl. Phys. Lett.*, **99** (2011) 091903.
12. Y.X. Xu, L. Chen, F. Pei, J.L. Yue, Y. Du, "Thermal stability and oxidation resistance of V-alloyed TiAlN coatings", *Ceram Int.*, **44** (2018) 1705–1710.
13. L. Rogström, M.P. Johansson-Jõesaar, R. Pilemalm, N. Ghafoor, L. Johnson, N. Schell, M. Odén, "Decomposition routes and strain evolution in arc deposited TiZrAlN coatings", *J. Alloy Compd.*, **779** (2019) 261–269.
14. A. Knutsson, M.P. Johansson, L. Karlsson, M. Odén, "Thermally enhanced mechanical properties of arc evaporated $Ti_{0.34}Al_{0.66}N$/TiN multilayer coatings", *J. Appl. Phys.*, **108** (2010) 044312.
15. Y.X. Xu, L. Chen, F. Pei, Y. Du, "Structure and thermal properties of TiAlN/CrN multilayered coatings with various modulation ratios", *Surf. Coat. Technol.*, **304** (2016) 512–518.
16. K.M. Calamba, I.C. Schramm, M.P. Johansson-Jõesaar, J. Ghanbaja, J.F. Pierson, F. Mücklich, M. Odén, "Enhanced thermal stability and mechanical properties of nitrogen deficient titanium aluminum nitride ($Ti_{0.54}Al_{0.46}N_y$) thin films by tuning the applied negative bias voltage", *J. Appl. Phys.*, **122** (2017) 065301.
17. S. Yousefi, M. Zohoor, "Effect of cutting parameters on the dimensional accuracy and surface finish in the hard turning of MDN250 steel with cubic boron nitride tool, for developing a knowledged base expert system", *Int. J. Mech.*

Mater. Eng., **14** (2019) 1.
18. S.N. Monteiro, A.L. Diegues Skury, M.G. de Azevedo, G.S. Bobrovnitchii, "Cubic boron nitride competing with diamond as a superhard engineering material - an overview", *J. Mater. Res. Tech.*, **2** (2019) 68–74.
19. B. Alling, A.V. Ruban, A. Karimi, O.E. Peil, S.I. Simak, L. Hultman, I.A. Abrikosov, "Mixing and decomposition thermodynamics of c-$Ti_{1-x}Al_xN$ from first-principles calculations", *Phys. Rev. B*, **75** (2007) 045123.
20. P.H. Mayrhofer, D. Music, J.M. Schneider, "Ab initio calculated binodal and spinodal of cubic $Ti_{1-x}Al_xN$", *Appl. Phys. Lett.*, **88** (2006) 071922.
21. N. Norrby, H. Lind, G. Parakhonskiy, M.P. Johansson, F. Tasnádi, L.S. Dubrovinsky, N. Dubrovinskaia, I.A. Abrikosov, M. Odén, "High pressure and high temperature stabilization of cubic AlN in $Ti_{0.60}Al_{0.40}N$", *J. Appl. Phys.*, **113** (2013) 053515.
22. A. Wang, S. Shang, Y. Du, L. Chen, J. Wang, Z. Liu, "Effects of pressure and vibration on the thermal decomposition of cubic $Ti_{1-x}Al_xN$, $Ti_{1-x}Zr_xN$, and $Zr_{1-x}Al_xN$ coatings: A first-principles study", *J. Mater. Sci.*, **47** (2012) 7621–7627.
23. N. Shulumba, O. Hellman, Z. Raza, B. Alling J. Barrirero, F. Mücklich, I.A. Abrikosov, M. Odén, "Lattice vibrations change the solid solubility of an alloy at high temperatures", *Phys. Rev. Lett.*, **117** (2016) 205502.
24. P. Cloudhary, J. Bellare, "Manufacture of gem quality diamonds: A review", *Ceram. Int.*, **26** (2000) 73–85.
25. R.C. Liebermann, "Multi-anvil, high pressure apparatus: a half-century of development and progress", *High Press. Res.*, **31** (2011) 493–532.
26. H.T. Hall, "Ultra-high-pressure, high-temperature apparatus: The "Belt"", *Rev. Sci. Instrum.*, **31** (1960) 125–131.
27. R.M. Langford, A.K. Petford-Long, "Preparation of transmission electron microscopy cross-section specimens using focused ion beam milling", *J. Vac. Sci. Technol. A*, **19** (2001) 2186–2193.
28. W.C. Oliver, G.M. Pharr, "An improved technique for determining hardness and elastic modulus using load and displacement sensing indentation experiments", *J. Mater. Res.*, **7** (1992) 1564–1583.
29. A.O. Eriksson, J.Q. Zhu, N. Ghafoor, M.P. Johansson, J. Sjölen, J. Jensen, M. Odén, L. Hultman, J. Rosén, "Layer formation by resputtering in Ti-Si-C hard coatings during large scale cathodic arc deposition", *Surf. Coat. Technol.*, **205** (2011) 3923–3930.
30. M. Adamik, P.B. Barna, I. Tomov, "Columnar structures in polycrystalline thin films developed by competitive growth", *Thin Solid Films*, **317** (1998) 64–68.
31. D.J. Srolovitz, A. Mazor, B.G. Bukiet, "Analytical and numerical modeling of columnar evolution in thin films", *J. Vac. Sci. Technol. A*, **6** (1988) 2371–2380.
32. S. Hoffman, S.T. Norberg, M. Yoshimura, "Melt synthesis of Al_2TiO_5 containing composites and reinvestigation of the phase diagram Al_2O_3-TiO_2 by powder X-ray diffraction", *J. Electroceram.*, **16** (2006) 327–330.
33. L. Rogström, J. Ullbrand, J. Almer, L. Hultman, B. Jansson, M. Odén, "Strain evolution during spinodal decomposition of TiAlN thin films", *Thin Solid Films*, **520** (2012) 5542–5549.
34. P.H. Mayrhofer, A. Hörling, L.J. Karlsson, J. Sjölen, T. Larsson, C. Mitterer, L. Hultman, "Self-organized nanostructures in the Ti-Al-N system", *Appl. Phys. Lett.*, **83** (2003) 2049–2051.
35. A. Nemati, M. Saghafi, S. Khamseh, E. Alibakhshi, P. Zarrintaj, M.R. Saeb, "Magnetron-sputtered Ti_xN_y thin films applied on titanium-based alloys for medical applications: Composition-microstructure-property relationships", *Surf. Coat. Technol.*, **349** (2018) 251–259.
36. A. Knutsson, J. Ullbrand, L. Rogström, N. Norrby, L.J.S. Johnson, L. Hultman, J. Almer, M.P. Johansson Jöesaar, B. Jansson, M. Odén, "Microstructure evolution during the isostructural decomposition of TiAlN – A combined in-situ small angle x-ray scattering and phase field study", *J. Appl. Phys.*, **113** (2013) 213518.
37. S. Sveen, J.M. Andersson, R. M'Saoubi, M. Olsson, "Scratch adhesion characterstics of PVD TiAlN deposited on high speed steel, cemented carbide and PCBN substrates", *Wear*, **308** (2013) 133–141.
38. J. Angseryd, E. Coronel, M. Elfwing, E. Olsson, H. Andrén, "The microstructure of the affected zone of a worn PCBN cutting tool characterised with SEM and TEM", *Wear*, **267** (2009) 1031–1040.
39. A.S. Manokhin, S.A. Klimenko, S. An Klimenko, V.M. Beresnev, "Promising types of coatings for PCBN tools", *J. Superhard Mater.*, **40** (2018) 424–431.